Journal of Nuclear Materials 442 (2013) S119–S214–S218
DOI: http://dx.doi.org/10.1016/j.jnucmat.2012.10.033

Influence of processing route and yttria additions on the oxidation behavior of tungsten

S.C. Cifuentes [a], A. Muñoz [b], M.A. Monge [b], P. Pérez [a,*]

[a] Departamento de Metalurgia Física, Centro Nacional de Investigaciones Metalúrgicas (CENIM-CSIC), Avd. Gregorio del Amo 8, 28040 Madrid, Spain
[b] Departamento de Física, Universidad Carlos III, Avda. Universidad 30, 28911 Leganés, Spain

Abstract: The oxidation resistance in dry air of pure tungsten and tungsten reinforced with a dispersion of 0.6 wt.%Y_2O_3 nanoparticles has been evaluated between 873 and 1073 K, temperature range that divertor in fusion power plants should endure during long-term times in the case of loss of coolant accident and/or air ingress in the vessel. Both materials were prepared by a powder metallurgy route involving hot iso-static pressing of ball milled tungsten powders and tungsten with dispersed Y_2O_3 nanoparticles. The results have been compared with those of pure tungsten processed by conventional techniques. Thermo-gravimetric tests at 873 K revealed that the processing route as well as yttria addition considerably affected the oxidation resistance of pure tungsten. Mass gain of W–0.6Y_2O_3 at 873 K was five and two times lower than that of pure tungsten prepared by conventional processing techniques and by powder metallurgy, respectively. This different behavior was related to changes in the structure and composition of the oxide scale. Above 873 K, the kinetics were significantly accelerated for all materials due to the development of a non-protective oxide scale from the earliest oxidation stages, although the kinetics of Y_2O_3-containing material were still the slowest, specially at 973 K. It was analyzed how yttria additions modify the oxidation mechanism of tungsten.

1. Introduction

The selection of plasma facing materials (PFMs) is a critical issue for the development of future fusion power plants [1,2]. It is well established that tungsten has many special advantages as material for plasma facing armour or shield components, such as: high melting point and very low vapor pressure, low sputtering yield, good thermal conductivity, low thermal expansion coefficient, high strength at high temperatures, low retention of tritium and good dimensional stability under neutron irradiation. The designs of the ITER divertor vertical targets and the DEMO helium cooled divertor first wall consider tungsten as the preference candidate material [3].

However, a major drawback of tungsten is its poor oxidation resistance [4,5] in case of Loss of Coolant Accident (LOCA) and air ingress as a result of failure of the vacuum vessel's integrity. The oxide scale on tungsten presents poor protective properties even at moderate temperatures of ~773 K [6]. After a LOCA incident the temperature of the plasma facing components will remain at higher temperatures for several weeks due to the large heat decay of the PFMs [7]. Therefore, the oxidation resistance of tungsten should be improved to ensure total safety of W-based plasma facing components in case of the accident scenarios described above.

The present work reports how tungsten processing by a powder metallurgical route and yttria additions affect the oxidation resistance of tungsten in dry air between 873 and 1073 K. The results are compared to previous oxidation data for ITER-reference tungsten grade [8] and commercial pure tungsten of different sources [6,9,10].

2. Experimental procedure

Pure tungsten prepared by powder metallurgy (W–PM) and Y_2O_3-reinforced tungsten (W–0.6Y_2O_3) were prepared from high purity W (99.9%) and Y_2O_3 (99.5%) powders with particle sizes below 5 μm and 30 nm, respectively. The preparation and sintering of the powders was done by following a four stages process: (1) blending of the starting powders in a Turbular T2F mixer for 4 h; (2) mechanical alloying of the powder blend for 20 h at 400 rpm in a high-energy planetary ball mill; (3) encapsulation, and degassing for 24 h at 673 K; and (4) sintering by hot isostatic pressing (HIP) for 2 h at 1573 K and 195 MPa. The resulting sintered materials were obtained as cylinder billets with nominal dimensions of ~30 mm diameter and ~50 mm length. The microstructural characterization and the mechanical properties of these materials in

* Corresponding author. Tel.: +34 915538900x211; fax: +34 915347425.
E-mail address: zubiaur@cenim.csic.es (P. Pérez).

the temperature interval 298–1273 K have been reported elsewhere [11,12].

Oxidation tests at 873 and 973 K were carried out on prismatic samples with $8 \times 8 \times 2$ mm^3. Tests at 1073 K were carried out on samples with nominal sizes $5 \times 5 \times 2$ mm^3. All major surfaces were abraded on successively finer silicon carbide papers, then mechanically polished with 1 μm diamond paste and cleaned with ethanol. Determination of the oxidation kinetics was carried out by continuous isothermal thermogravimetry tests in the temperature range 873–1073 K for exposures up to 100 h. At 1073 K, exposure time was reduced to 20 h because the high mass gain of the samples implied the risk of exceeding the maximum weight range of the microbalance. Oxidation tests were carried out under dry synthetic air (dewpoint below 233 K).

Characterization of oxidation products was performed on samples used for mass-gain determination as well as on samples isothermally oxidized for different exposure times. Cross-sections were prepared by conventional metallographical techniques. To prevent scale loss during the metallographic preparation of the sample, the surfaces were successively coated first with a thin gold layer (by sputtering) and then with a thicker layer of copper (electrolytically deposited). Surfaces and cross-sections of the oxidized specimens were studied by scanning electron microscopy (SEM). Phase identification of the oxide scale was performed from X-ray diffraction (XRD) patterns obtained with K_αCo radiation and from energy dispersive X-ray microanalysis (EDX).

3. Results and discussion

Fig. 1 plots mass gain versus time for W–PM and W–0.6Y_2O_3 at 873, 973 and 1073 K. As reference, the mass gain curve for pure W (W–CP) of a ITER-reference tungsten grade, 99.97% purity, is shown (for more detail see Ref. [8]). Mass gain curves proved that oxide scale formed on these materials conferred protection only at 873 K, being non-protective above this temperature. Major differences in mass gain curves were noticed at 873 and 973 K. Thus, after 100 h exposure at 873 K, the mass gain of W–0.6Y_2O_3, 4 mg/cm^2, was almost one-third that of W–CP (11.3 mg/cm^2) and two-thirds that of W–PM (6.6 mg/cm^2).

Once more, at 973 K, the lower mass gain over the entire exposure corresponded to the yttria-containing alloy. Mass gain increased rapidly during the earliest oxidation stages for W–CP compared with the relatively slow increase observed for W–PM and W–0.6Y_2O_3 in the first 10 h of exposure. However, the mass gain rate tended to diminish gradually for W–CP with progressing oxidation while this decrease was less pronounced for W–PM and W–0.6Y_2O_3. Thus, mass gain after 100 h exposure was lower for W–CP (135 mg/cm^2) than for W–PM (152 mg/cm^2). In the case of W–0.6Y_2O_3, the mass gain was the lowest one during the whole exposure (129 mg/cm^2).

At 1073 K, all materials experienced a high mass gain rate, as shown in Fig. 1c. Hence, after 20 h of exposure mass gain was practically the same, even higher in the case of W–0.6Y_2O_3, of that measured during exposure at 973 K for 100 h. Fig. 1c shows the rapid changes in the oxidation rate, reproducing at shorter exposures the tendency observed at 973 K. Although the mass gain of W–CP was initially the highest, after further exposure up to 20 h the mass gain of W–CP, 141 mg/cm^2, became lower than that of W–PM and W–0.6Y_2O_3, showing mass gains of 155 and 177 mg/cm^2, respectively.

XRD patterns detected intense WO_3 peaks in all materials irrespective the oxidation temperature. Additional peaks corresponding to W_5O_{14}, $W_{18}O_{49}$ and Y_2WO_6 (the last oxide formed during hipping stage of the processing route) were found in XRD patterns of W–0.6Y_2O_3 after exposure at 873 K for 100 h.

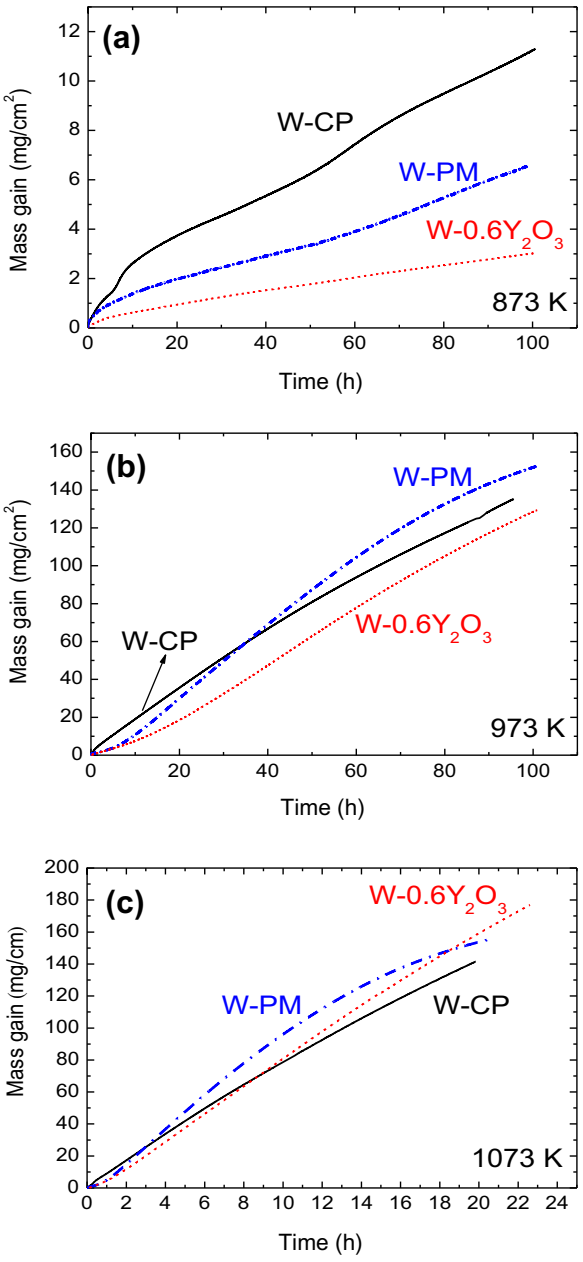

Fig. 1. Mass gain curves of W–CP, W–PM and W–0.6Y_2O_3. (a) 873 K, (b) 973 K and (c) 1073 K.

Surface views of the oxidized layers showed some differences in the morphology of the external oxide scale, as shown in Fig. 2 for the materials oxidized at 873 K. Thus, the outermost layer formed on W–CP consisted of round fine-grained oxide particles. A more geometrical structured oxide with a larger size was found on the surface of the oxide developed on W–PM. The coarsest size of oxide grains was found on W–0.6Y_2O_3.

The grain size of the outermost oxide layer increased with increasing oxidation temperature for W–CP and W–PM but not for W–0.6Y_2O_3, as shown in Fig. 3. Although the exposure was only 20 h at 1073 K, the faster growth of the oxide grain size with temperature was observed for the W–PM, which has the coarsest grains at 1073 K. This figure also evidenced that the outermost part of the scale developed at 1073 K was very similar in all materials when a non-protective layer was formed.

Cross sectional views provided more precise information about the scales. Major differences were found in the scale developed at

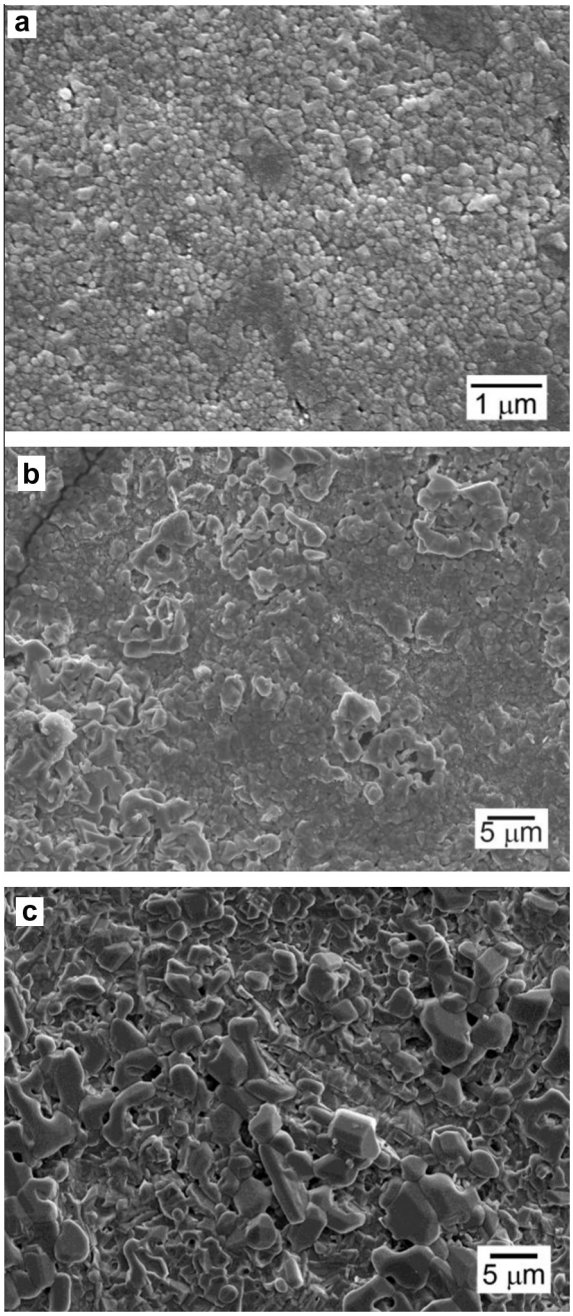

Fig. 2. Surface of the samples oxidized 100 h at 873 K. (a) W–CP, (b) W–PM and (c) W–0.6Y_2O_3.

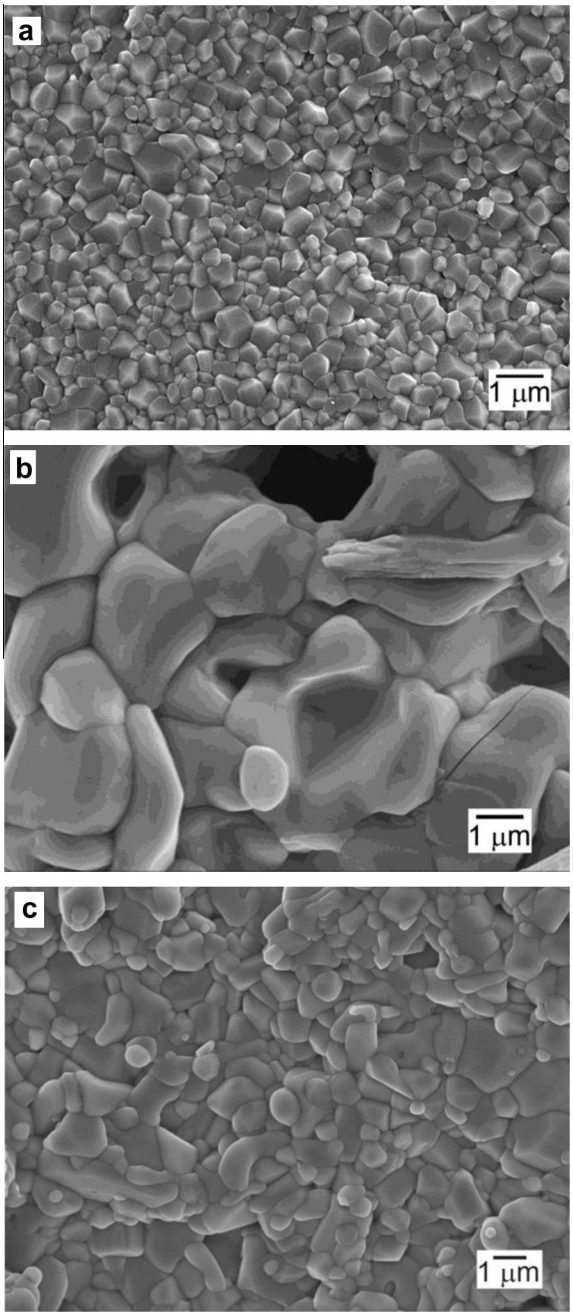

Fig. 3. Surface of the samples oxidized 20 h at 1073 K. (a) W–CP, (b) W–PM and (c) W–0.6Y_2O_3.

873 K. At this temperature, the thickness and structure of the oxide scale significantly changed depending on the material, as shown in Fig. 4. In agreement with mass gain curves, maximum thickness corresponded to W–CP, about 95 μm and minimum to W–0.6Y_2O_3, about 18 μm. Thickness of the scale on W–PM was not uniform, presenting thin dense regions of about 20 μm, similar to that observed in W–0.6Y_2O_3, and thick regions of about 75 μm whose microstructure resembled rather well that found in W–CP [8]. The oxide scale formed on W–CP consisted of two layers, clearly depicted by a nearly continuous band of cavities between both layers (see Fig. 4a). The thin dense outermost layer was about 10 μm and the thicker innermost layer was about 85 μm, with a stratified microstructure consisting of alternating dense and porous regions. Either cracks running throughout the oxide scale from the oxide/metal interface to the gas/oxide interface or cracks running parallel to the oxide/metal interface could be observed. The absence of localized attack ahead of the crack tip proved that accelerated oxide growth could not be associated with transverse cracking. Probably transverse cracks were generated during cooling down. Parallel cracks, however, could be generated by the significant volume change resulting from the oxidation of tungsten into WO_3 (3.3 as Pilling–Bedworth ratio). Growth stresses stored in the scale were released during cracking events. Microcracking turned the initially protective layer in a non-protective scale in which oxygen can ingress rapidly into the material, changing the kinetics from parabolic to linear [6].

The scale developed in W–0.6Y_2O_3 was more compact. Nevertheless, the scale was also divided into two parts, as found in W–CP: A thin outermost dense layer of about 3.5 μm and a thicker innermost layer of about 15 μm (see Fig. 4c). Some isolated poros-

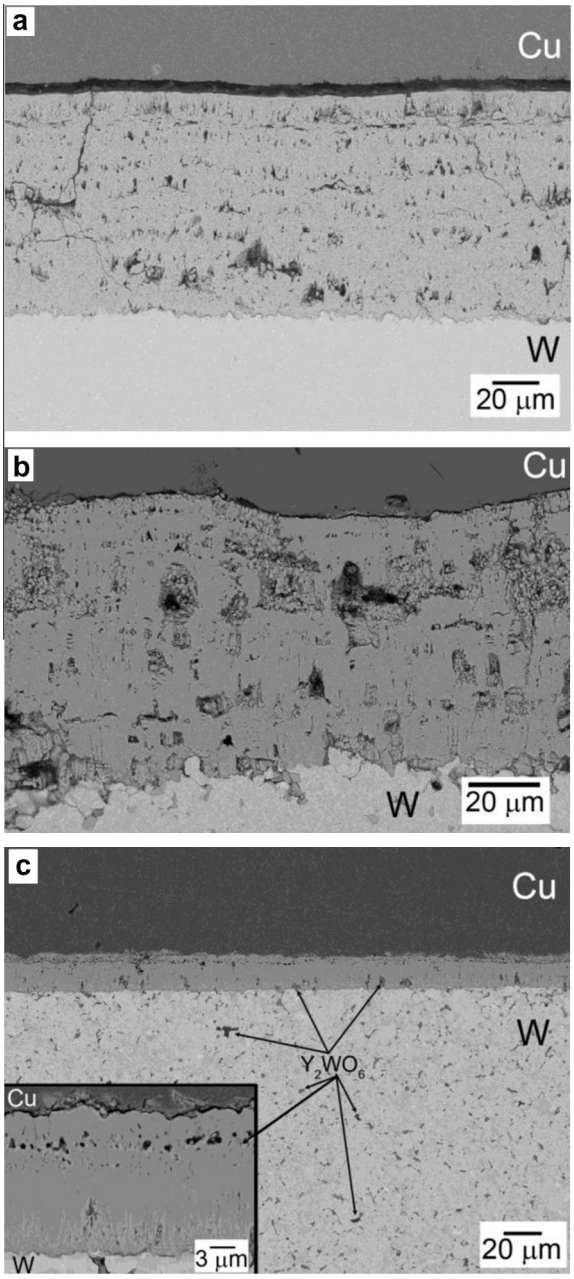

Fig. 4. Cross sectional views of the scales formed after 100 h exposure at 873 K. (a) W–CP, (b) W–PM and (c) W–0.6Y_2O_3. The inset shows a close magnification of the scale.

ity is aligned along the interface between both layers. Moreover, porosity was not as abundant as in the innermost layer formed in W–CP. In addition, some thick Y_2WO_6 particles were embedded in the scale, indicating that oxidation proceeded by inward oxygen transport into the alloy, as reported by other authors [13]. Absence of parallel cracks suggested that cracking was hindered in the yttria-containing material, leading to a significant decrease in the mass gain. As a consequence other more protective oxides, i.e. W_5O_{14} and $W_{18}O_{49}$, can be formed, as detected in XRD patterns, because oxygen partial pressure at the scale/metal interface is not raised by cracking. These results suggest that yttria additions might modify the stress state in the scale, delaying the cracking stage for longer exposure times that in the scale established in W–CP. In the case of W–PM, the outermost thin layer of the scale behave similar to the scale developed in W–0.6Y_2O_3, while the innermost thick part of the scale was generated in a similar way to that established on W–CP [8].

As the oxidation temperature was raised, differences in the structure of the oxide scale were minimized, as presented in Fig. 5. At 973 and 1073 K, thick scales with a stratified structure grew in all materials, up to 1.6 mm in thickness for W–PM oxidized at 973 K for 100 h. The stratified structure is similar to that reported during oxidation of pure titanium in air [14]. Unlike rutile scale formed on titanium, each individual layer/stratum was separated from adjacent layers by interconnected cavities instead of a continuous cracking. This suggests that oxide growth stresses, leading to the formation of each individual layer, are released by

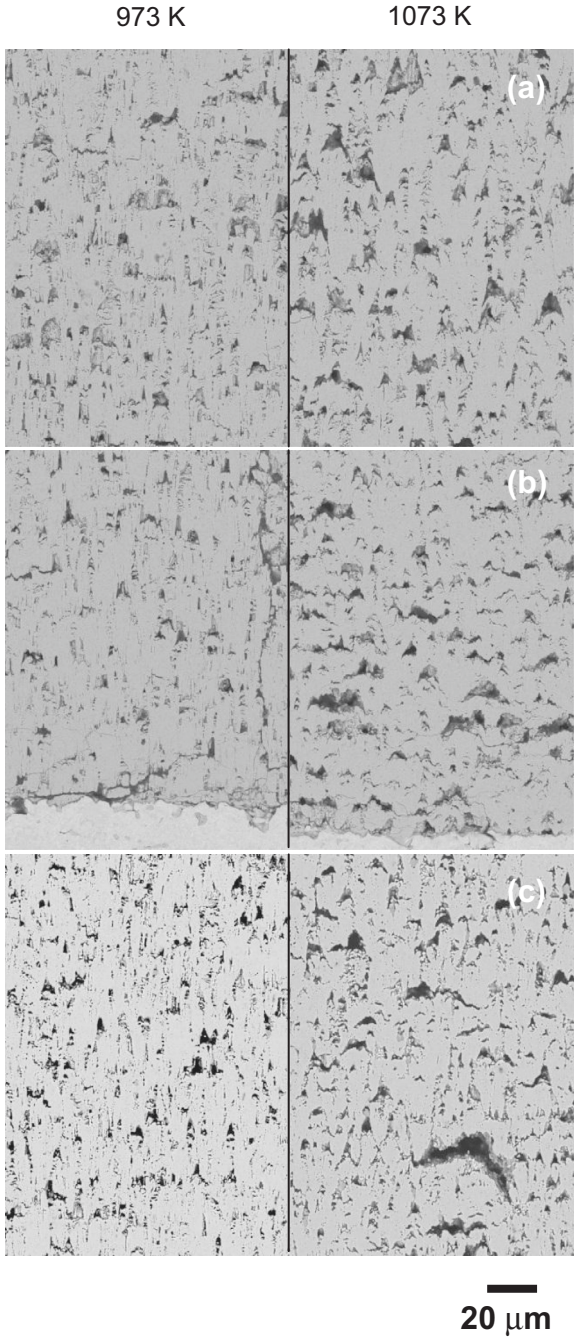

Fig. 5. Cross sections of the scales developed in dry air at 973 and 1073 K on: (a) W–CT, (b) W–PM and (c) W–0.6Y_2O_3. The exposure was 100 h at 973 K and 20 h at 1073 K.

multiple microcracking events and not by a single cracking event. The oxidation mechanism on pure tungsten has been reviewed by Cifuentes et al. [8]. Basically, the oxidation proceeded through a cyclic mechanism involving periodic cracking at local areas when a dense oxide layer attained a critical thickness. Cracked areas constituted an obstacle to inward oxygen diffusion, so oxidation proceeded faster in metal adjacent to the crack, where new oxide is formed. The large volume increase associated with new oxide formation shifted the scale outwards in such a way that the crack is progressively transformed into a cavity. The development of the stratified scale in W–0.6Y_2O_3, indicated that yttria additions were not effective in reducing oxidation kinetics of tungsten at 973 and 1073 K. Oxidation kinetics did not follow linear laws only during short-term exposure at 973 K for the W–PM and W–0.6Y_2O_3. Probably, in this period a relatively protective oxide, $W_{18}O_{49}$ and/or W_5O_{14} could be formed. Theses oxides, however, would not form further once cracking of the scale took place as result of large growth stresses, leading to linear kinetics.

4. Conclusions

During short-term exposures at lower temperatures, yttria additions increase microcracking resistance of the oxide scale so a normal oxygen gradient is established across the scale. This allowed the formation of other more protective oxides, $W_{18}O_{49}$ and W_5O_{14}, which were absent in the scales formed on yttria-free tungsten. Beneficial effect of yttria additions was restricted to 873 K but disappeared at higher temperatures because of microcracking in the oxide scale. At 973 and 1073 K, the oxidation mechanism was identical in all materials, resulting in the formation of a non-protective stratified layer.

Acknowledgements

The present work has been supported by the Consejería de Educación de la Comunidad de Madrid through the program ESTRUMAT-CM S2009MAT-1585 and by the Ministerio de Innovación y Ciencia (Project ENE2008-06403-C06-04). The additional subvention from EURATOM/CIEMAT association through contract EFDA WP11-MAT-WWALLOY is also acknowledged.

References

[1] J. Pamela, A. Becoulet, D. Borba, J.L. Boutard, L. Horton, D. Maisonnier, Fusion Eng. Des. 84 (2009) 194–204.
[2] S.J. Zinkle, Fusion Eng. Des. 74 (2005) 31–40.
[3] M. Rieth, J.L. Boutard, S.L. Dudarev, T. Ahlgren, S. Antusch, N. Baluc, M.F. Barthe, C.S. Becquart, L. Ciupinski, J.B. Correia, C. Domain, J. Fikar, E. Fortuna, C.C. Fu, E. Gaganidze, T.L. Galán, C. García-Rosales, B. Gludovatz, H. Greuner, K. Heinolas, N. Holsteina, N. Juslins, F. Kochp, W. Kraussa, K.J. Kurzydlowskie, J. Linked, Ch. Linsmeierp, N. Luzginovai, H. Maierp, M.S. Martínez, J.M. Missiaen, M. Muhammed, A. Muñoz, M. Muzyk, K. Nordlund, D. Nguyen-Manh, P. Norajitra, J. Opschoor, G. Pintsuk, R. Pippan, G. Ritz, L. Romaner, D. Rupp, R. Schäublin, J. Schlosser, I. Uytdenhouwen, J.G. van der Laan, L. Veleva, L. Ventelon, S. Wahlberg, F. Willaime, S. Wurster, M.A. Yar, J. Nucl. Mater. 417 (2011) 463–467.
[4] G.A. Cottrell, Mater. Sci. Technol. 22 (2006) 869–880.
[5] V. Tang, R.R. Parker, Fusion Eng. Des. 65 (2003) 11–26.
[6] E.A. Gulbransen, K.F. Andrew, J. Electrochem. Soc. 107 (1960) 619–628.
[7] J. Roth, E. Tsitrone, A. Loarte, Nucl. Instrum. Meth. B 258 (2007) 253–263.
[8] S.C. Cifuentes, M.A. Monge, P. Perez, Corros. Sci. 57 (2012) 114–121.
[9] W.W. Webb, J.T. Norton, C. Wagner, J. Electrochem. Soc. 103 (1956) 107–111.
[10] E.A. Kellet, S.E. Rogers, J. Electrochem. Soc. 110 (1963) 502–504.
[11] M.A. Monge, M.A. Auger, T. Leguey, Y. Ortega, L. Bolzoni, E. Gordo, J. Nucl. Mater. 386 (2009) 613–617.
[12] M.V. Aguirre, A. Martin, J.Y. Pastor, J. Llorca, M.A. Monge, R. Pareja, Metall. Mater. Trans. A 40 (2009) 2283–2290.
[13] V.K. Sikka, C.J. Rosa, Corros. Sci. 20 (1980) 1201–1219.
[14] P. Pérez, G. Salmi, A. Muñoz, M.A. Monge, Scripta Mater. 60 (2009) 1008–1011.